Chemistry Europe
European Chemical Societies Publishing

VIP $Cs_4B_4O_3F_{10}$: First Fluorooxoborate with $[BF_4]$ Involving Heteroanionic Units and Extremely Low Melting Point

Ming Xia,[a, b] Miriding Mutailipu,*[a, b] Fuming Li,[a, b] Zhihua Yang,[a, b] and Shilie Pan*[a, b]

Abstract: Herein, a new congruently melting mixed-anion compound $Cs_4B_4O_3F_{10}$ has been characterized as the first fluorooxoborate with $[BF_4]$ involving heteroanionic units. Compound $Cs_4B_4O_3F_{10}$ possesses two highly fluorinated anionic clusters and therefore its formula can be expressed as $Cs_3(B_3O_3F_6)\cdot Cs(BF_4)$. The influence of $[BF_4]$ units on microsymmetry and structural evolution was discussed based on the parent compound. More importantly, $Cs_4B_4O_3F_{10}$ shows the lowest melting point among all the available borates and thus sets a new record for such system. This work is of great significance to enrich and tailor the structure of borates using perfluorinated $[BF_4]$ units.

The introduction of multiple anions can facilitate the discovery of novel compounds with extended solid state chemistry and unique properties, which has led to the significant advances in wide fields such as chemistry, energy, and materials, etc.[1] Oxyfluoride is such a case, which can be regarded as the derivative of partly substituting oxygen with fluorine.[1c] To an extent, this process not only offers a new handle to regulate the properties, but also provides novel chromophores to construct the high-performing optical materials.[1]

Among them, the introduction of fluorine into borates to construct fluorooxoborates is proved to be an effective approach to extend the solid state chemistry and to push the current limitations of borate-based optical materials.[2a,b] The fluorinated anionic units in fluorooxoborates are beneficial for broadening the energy bandgap, reducing the symmetry, improving the hyperpolarizability, and enhancing the polarizability anisotropy owing to large electronegativity of fluorine when compared with oxygen.[2,3] Therefore, many fluorooxoborates have been synthesized and characterized with novel structures and properties in a few short years,[2a,b,3–6] which provides new fertile fields for expanding the solid state chemistry and functionality of borate system.[7,8] For example, $Li_2B_3O_4F_3$ and BiB_2O_4F are the only fluorooxoborates with fluorinated anionic chains, that is, $^1[B_3O_4F_3]_\infty$ and $^1[B_6O_{10}F_2]_\infty$ chains.[5d,e] AB_4O_6F (A=NH_4, Na, Rb, Cs) and $MB_5O_7F_3$ (M=Ca, Sr, Mg) series are the most promising candidates for deep-UV nonlinear optical applications.[4] More importantly, several unprecedented heteroanionic units have been observed in fluorooxoborate system like $[B_4O_6F_4]$,[5a] $[B_5O_9F_3]$,[4e,f] $[B_5O_{10}F]$,[5c] $[B_7O_{13}F_2]$,[5b] and $[B_{10}O_{12}F_{13}]$ groups,[6a] which is found in no other related oxyfluorides.

However, the number of fluorooxoborates is extremely limited when compared with pure borates (more than 3900) and only less than 50 anhydrous cases belong to this species.[2a] As yet, the existence of perfluorinated $[BF_4]$ units in fluorooxoborates remains experimentally unknown, although this is very common in tetrafluoroborates where their anionic frameworks solely consist of boron-fluorine anions.[9a,b] It should be noted that the perfluorinated $[BF_4]$ units can be seen as the derivatives of $[BO_4]$ units where all the oxygen are completely replaced by fluorine, which show largest energy bandgap in B–O/F modules according to the theoretical analysis.[2a] In addition, unlike $[BO_4]$ unit, the $[BF_4]$ unit can only be in isolated configuration and is beneficial for reducing the dimension of anionic framework. With this in mind, $Cs_4B_4O_3F_{10}$, the first fluorooxoborate with $[BF_4]$ involving heteroanionic units has been synthesized, which is the second case of possessing two types of isolated fluorinated anionic clusters. Symmetry analysis confirms the roles of perfluorinated $[BF_4]$ units on symmetry breaking based on its parent compound, $Cs_3(B_3O_3F_6)$. More importantly, the title compound exhibits congruent melting behavior and therefore millimeter scale single crystals can be easily grown. Besides, the more detailed experimental and theoretical analyses have also been studied to clarify the structure-property relationship.

$Cs_4B_4O_3F_{10}$ crystals can be grown by high-temperature solution method in a closed or open system using the B_2O_3 flux or under its stoichiometry (see detail in the following experimental section). Polycrystalline sample of $Cs_4B_4O_3F_{10}$ was obtained by solid-state reaction or by grinding the above as-grown single crystals (Figure 1a). The single crystal and powder XRD analyses confirmed the crystal structure and phase purity, respectively (Figure 1a). Figure 1b presents the thermal gravimetric analysis (TGA) and differential scanning calorimetry (DSC), in which there are two endothermic peaks at about 293 and 322 °C on the heating curve without any weight loss on the TG curve. But there are no any detectable exothermic peaks on

[a] M. Xia, Prof. M. Mutailipu, F. Li, Prof. Z. Yang, Prof. S. Pan
CAS Key Laboratory of Functional Materials and Devices for Special Environments
Xinjiang Technical Institute of Physics and Chemistry, Chinese Academy of Sciences
Xinjiang Key Laboratory of Electronic Information Materials and Devices
40-1 South Beijing Road, Urumqi 830011 (P.R. China)
E-mail: miriding@ms.xjb.ac.cn
slpan@ms.xjb.ac.cn

[b] M. Xia, Prof. M. Mutailipu, F. Li, Prof. Z. Yang, Prof. S. Pan
Center of Materials Science and Optoelectronics Engineering
University of Chinese Academy of Sciences
Beijing 100049 (P.R. China)

Supporting information for this article is available on the WWW under https://doi.org/10.1002/chem.202101321

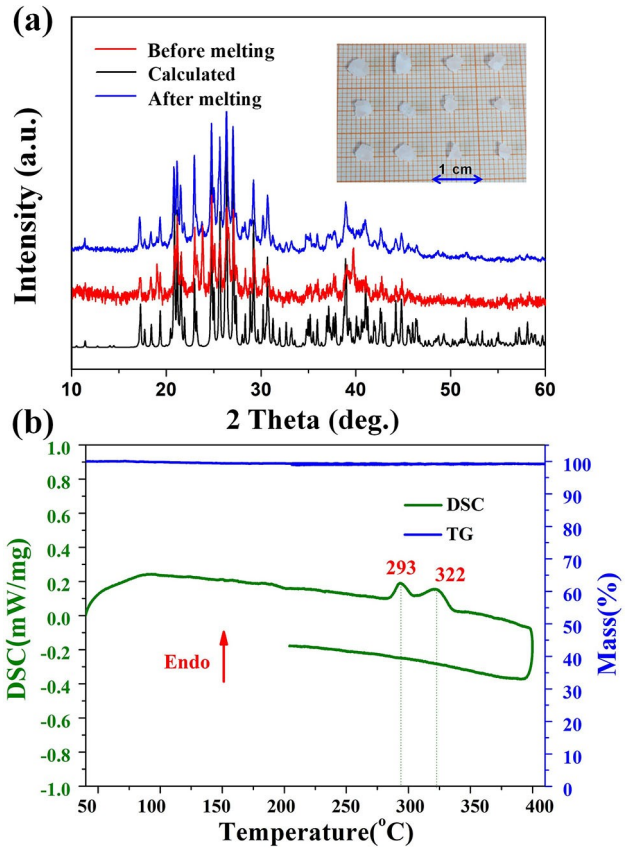

Figure 1. (**a**) Experimental and calculated XRD patterns of $Cs_4B_4O_3F_{10}$, insert gives the photograph of as-grown single crystals. (**b**) TG-DSC curves of $Cs_4B_4O_3F_{10}$.

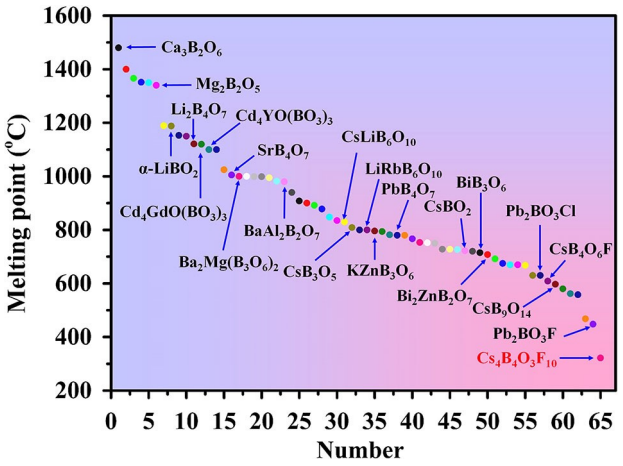

Figure 2. The melting points of available congruently melting borate. All the compounds are listed in Table S7 in the Supporting Information.

the cooling curve because of the high viscosity of $Cs_4B_4O_3F_{10}$ compound. Analysis of the powder XRD pattern of the solidified melt indicates that the entire residues exhibit a diffraction pattern identical to that of the initial polycrystalline samples, suggesting that $Cs_4B_4O_3F_{10}$ is a congruently melting compound. Thus, the two endothermic peaks might refer to the phase transition and melting point, respectively. Unfortunately, we have not obtained this low temperature phase, even though the quenching method was used. The reason may be that the phase transition is reversible. Even so, bulk $Cs_4B_4O_3F_{10}$ single crystals could, in principle, be grown under its stoichiometry with Czochralski and Kyropoulos techniques. More importantly, $Cs_4B_4O_3F_{10}$ shows the lowest melting point among all the available borates and thus sets a new record for borate system with congruently melting behavior. The melting points of all the available congruently melting borate are listed and summarized in Figure 2 based on the related literature data. Obviously, compounds with congruently melting behavior are extremely rare and their proportion is less than ~3% in borate system. Such a low melting point might come from the smaller formation energies of $Cs_4B_4O_3F_{10}$ (−5.91 eV) when compared with CsB_4O_6F (−7.59 eV), which requires lower energy to break the chemical bonds in related structures.

$Cs_4B_4O_3F_{10}$ crystallizes into monoclinic crystal system with a centrosymmetric space group $P2_1/c$ (No. 14; Table S1, Supporting Information).[10] As portrayed in Figures 3a and 3b, the structure of $Cs_4B_4O_3F_{10}$ features two alternately pseudo-layers composed of $[B_3O_3F_6]$ and $[BF_4]$ clusters with the sequence of –AA′BB′AA′– in (011) plane. These pseudo-layers are further stacked along the [100] direction with the monovalent Cs cation-based polyhedra located in the interlayer. The asymmetric unit of $Cs_4B_4O_3F_{10}$ contains four Cs, four B, three O, and ten F symmetrically independent atoms, respectively. (see Table S2, Supporting Information). All the B atoms have only one coordination model, four-coordinated tetrahedra with different fluorinated types of $[B(1,2,3)O_2F_2]$ and $[B(4)F_4]$ units (Figure 3a and Table S2, Supporting Information). The B–O and B–F bond lengths in $[BO_2F_2]$ tetrahedra vary from 1.412(6) to 1.431(6) Å and 1.431(5) to 1.461(6) Å, respectively, whereas the B–F bond lengths in $[B(4)F_4]$ units change from 1.339(8) to 1.377(7) Å (Tables S3 and S4, Supporting Information). These values agree well with those of other reported borates and fluorooxoborates.[2a,7,9] Every three $[BO_2F_2]$ units polymerize into a three-membered $[B_3O_3F_6]$ ring by sharing the bridged O(1,2,3) atoms. Both $[B_3O_3F_6]$ and $[BF_4]$ units are in isolated arrangement without further linking with the neighboring B atoms, and such a configuration is extremely rare in fluorooxoborates system and is only observed in isomorphic $A_{10}B_{13}O_{15}F_{19}$ (A=K, Rb)[6a] with isolated $[B_{10}O_{12}F_{13}]$ and $[B_3O_3F_6]$ units. Here we present the second example of possessing two different fluorinated B–O/F anionic units. To our knowledge, $Cs_4B_4O_3F_{10}$ is the first fluorooxoborate with perfluorinated $[BF_4]$ units and its formula can be expressed as $Cs_3(B_3O_3F_6)\cdot Cs(BF_4)$ according to its ionic salt nature, and therefore $Cs_4B_4O_3F_{10}$ powder can also be obtained by mixing $Cs_3(B_3O_3F_6)$ and $Cs(BF_4)$. For the cationic part, Cs(1) and Cs(2,3,4) are coordinated with O and F atoms to form $[Cs(1)F_6O_4]$, $[Cs(2)F_8O_2]$, and $[Cs(3,4)F_9O]$ polyhedra (Table S3, Supporting Information), respectively, which are further interconnected with $[B_3O_3F_6]$ and $[BF_4]$ units to form the final framework, shown in Figure 3b.

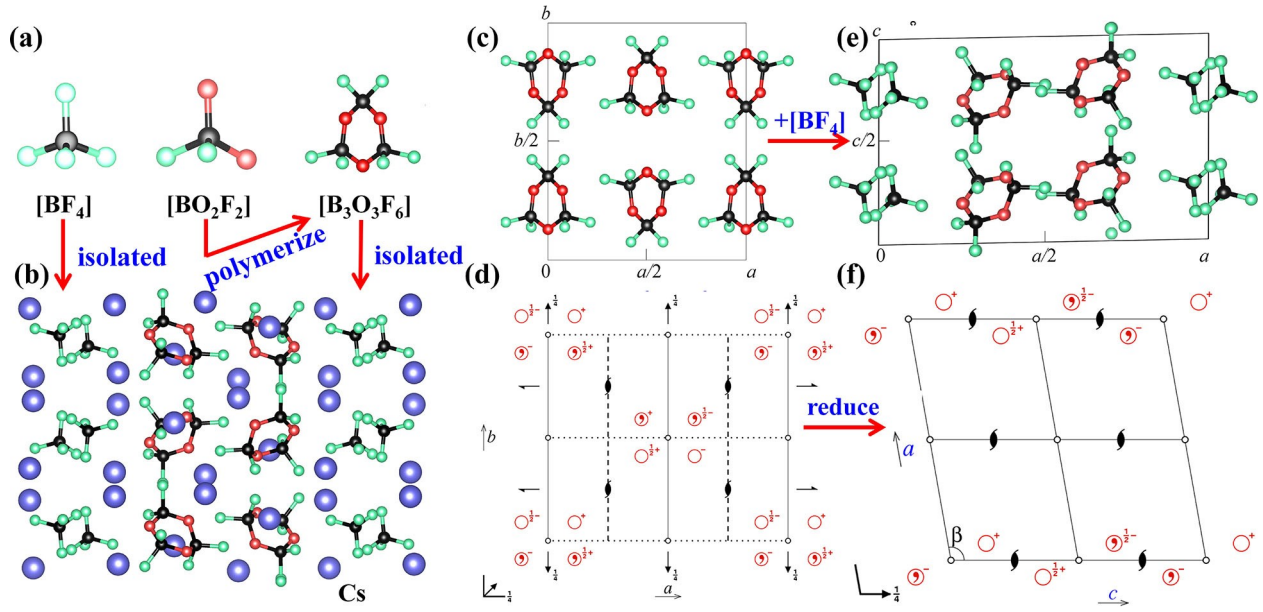

Figure 3. (**a**) The geometric configuration of $[BF_4]$, $[BO_2F_2]$, and $[B_3O_3F_6]$ units. (**b**) Crystal structure of $Cs_4B_4O_3F_{10}$ viewed in the (001) plane. (**c** and **e**) The anionic framework of $Cs_3(B_3O_3F_6)$ and $Cs_4B_4O_3F_{10}$. (**d** and **f**) The space group diagrams which show the positions of the symmetry elements of *Pbcn* and $P2_1/c$ within a single unit cell.

As was mentioned, the formula of $Cs_4B_4O_3F_{10}$ can also be written as $Cs_3(B_3O_3F_6)\cdot Cs(BF_4)$, thus, in this part, the influence of $[BF_4]$ units on micro-symmetry and also the structural evolution from $Cs_3(B_3O_3F_6)$ to $Cs_3(B_3O_3F_6)\cdot Cs(BF_4)$ were discussed. In contrast to $Cs_4B_4O_3F_{10}$, $Cs_3B_3O_3F_6$ crystallizes into the orthorhombic crystal system with the space group *Pbcn* (No. 61) and its structure is only composed of $[B_3O_3F_6]$-based pseudo-layers that are separated by Cs^+ cations.[6b] As shown in Figures 3d and 2f, the space group diagram of $P2_1/c$ indicates that $Cs_4B_4O_3F_{10}$ has the micro-symmetry elements including 2_1 helical axis and slip plane (SP) *c*, whereas $Cs_3B_3O_3F_6$ possesses three micro-symmetry elements, namely the mutually perpendicular SPs, namely *b*, *c* and *n*. In fact, the anionic part of $Cs_3B_3O_3F_6$ ($[B_3O_3F_6]$) and $Cs_4B_4O_3F_{10}$ ($[B_3O_3F_6]$ and $[BF_4]$), is sufficient to present the different micro-symmetric elements between them, thus their cations are omitted here for clarity. These projections of micro-symmetry elements were visually displayed in Figure S1 in the Supporting Information except the SP *n*, since it is a 3D micro-symmetric element here. Taking the anionic framework of $Cs_3B_3O_3F_6$ as the prototype, the strong polar $[BF_4]$ units are embedded into its lattice, resulting in the strong steric hindrance of two adjacent $[B_3O_3F_6]$ rings. In order to relieve the internal stress caused by $[BF_4]$ units, the $[B_3O_3F_6]$ rings undergo a greater distortion, which can be verified by the increased distorted dihedral angles from $<B_1B_2B_1{-}F_4> = 98.73^\circ$ in $Cs_3B_3O_3F_6$ to $<B_2B_1B_2{-}F_3> = 110.77^\circ$ in $Cs_4B_4O_3F_{10}$. At the same time, the number of crystallographic positions of B atoms in $[B_3O_3F_6]$ rings increase from two to three, indicating that the insert of $[BF_4]$ units into the lattice will reduce the local symmetry of $[B_3O_3F_6]$ rings. Thus, the $[BF_4]$ units break the original micro-symmetry operation of SP *b* in $Cs_3B_3O_3F_6$, then a new micro-symmetry element 2_1 helical axis is generated (Figure S1, Supporting Information). Similar to $Cs_3B_3O_3F_6$, the $[B_3O_3F_6]$ ring remains similar coordination configuration and thus a SP *c* micro-symmetry element has been reserved in $Cs_4B_4O_3F_{10}$. Therefore, the perfluorinated $[BF_4]$ tetrahedra can increase the distortion of $[B_3O_3F_6]$ rings because of the steric hindrance, which leads to the reduction of local symmetry from *Pbcn* (No. 61) in $Cs_3B_3O_3F_6$ to $P2_1/c$ (No. 14) in $Cs_4B_4O_3F_{10}$. This clearly indicates that the perfluorinated $[BF_4]$ units can be used to tailor the structure of borates.

The UV-vis-NIR diffuse reflectance spectrum data (Figure S2, Supporting Information) were collected based on the as-prepared polycrystalline sample, which indicates that $Cs_4B_4O_3F_{10}$ crystal can be transparent into deep-UV spectral region below 200 nm. Such a short cutoff edge of $Cs_4B_4O_3F_{10}$ attributes to the following two main factors from the viewpoint of micro-structure: (1) All the compositions including Cs, B, O, and F in $Cs_4B_4O_3F_{10}$ are free of *d–d* or *f–f* electronic transitions; (2) The non-bonding states of O atoms in anionic framework are effectively removed by the introduction of fluorine with the largest electronegativity. The IR spectrum and the related absorption peaks are presented in Figure S3 and Table S5 in the Supporting Information, which further confirms the existence of the B–F bonds in the structure of $Cs_4B_4O_3F_{10}$ with the formation of $[BF_4]$ and $[BO_2F_2]$ tetrahedra. In order to further explore the band structures of $Cs_4B_4O_3F_{10}$, the theoretical calculations were carried out based on DFT method, which shows that $Cs_4B_4O_3F_{10}$ is an indirect compound with the valence band maximum and conduction band minimum located in the different points. The calculated bandgaps using GGA and HSE06 methods are about 5.206 and 6.580 eV for $Cs_4B_4O_3F_{10}$, indicating that it can be transparent into the deep-UV spectral region (Figure 4a). Previous studies have shown that the electronic states near the

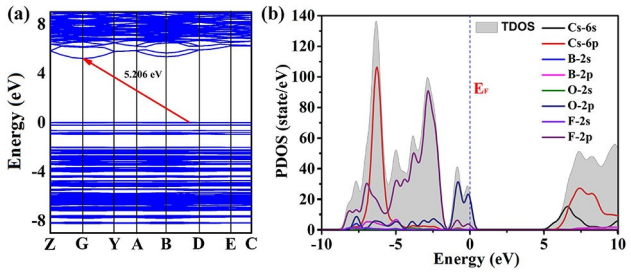

Figure 4. (**a**) Electronic band structure of $Cs_4B_4O_3F_{10}$ based on the results of GGA method. (**b**) The total and partial density of states of $Cs_4B_4O_3F_{10}$, in which E_F refers to Fermi level with energy of 0 eV.

Fermi level play a dominant role on the optical properties. Thus, we portrayed the density of states and it shows that the uppermost part of valence bands from −1.5 to 0 eV is essentially dominated by O 2p and F 2p states and a tiny contribution from Cs 6s orbitals can also be observed. Whereas for the bottom of conduction band, it is mainly composed of Cs 6s, Cs 6p and B 2p orbitals (Figure 4b). And the orbitals of F atoms are all far from the bottom of conduction band, indicating that the F atom with large electronegativity is beneficial for increasing the minimum of conduction band. When taken together, we can conclude that the Cs–O and B–O/F interactions play a decisive role in determining the bandgap of $Cs_4B_4O_3F_{10}$. The calculated energy bandgap of $Cs_4B_4O_3F_{10}$ (6.58 eV) is smaller than that of $Cs_3B_3O_3F_6$ (7.16 eV)[6b] using the same HSE06 method, which can be explained by the stronger ionic character of Cs components in $Cs_4B_4O_3F_{10}$ than that in $Cs_3B_3O_3F_6$. The involved states of Cs at conduction band make the minimum value shift to near the Fermi level, which will further decrease the bandgap.

In summary, $Cs_4B_4O_3F_{10}$, the first fluorooxoborate with $[BF_4]$ involving heteroanionic units has been synthesized and characterized. Structurally, $Cs_4B_4O_3F_{10}$ possesses two highly fluorinated anionic clusters, that is, $[B_3O_3F_6]$ and $[BF_4]$ units, which make it the second case with two types of isolated fluorinated anionic clusters. The before and after melting XRD curves of powder have demonstrated that the title compound is a concurrently melting compound. The influence of $[BF_4]$ units on microsymmetry and structural evolution based on the parent compound of $Cs_3B_3O_3F_6$ indicate that the perfluorinated $[BF_4]$ units can be used to tailor the structure of borates, which is of great significance to enrich structural chemistry of borates.

Experimental Section

Single crystal preparation and synthesis of title compounds: $Cs_4B_4O_3F_{10}$ crystals can be grown by high-temperature solution method in a closed or open system using the B_2O_3 flux or under its stoichiometry. Polycrystalline sample of $Cs_4B_4O_3F_{10}$ was obtained by solid-state reaction by grinding the above as grown single crystals. A mixture of $CsBF_4$ (0.201 g, 0.915 mmol), CsF (0.139 g, 0.915 mmol), B_2O_3 (0.032 g, 0.459 mmol) and H_3BO_3 (0.028 g, 0.459 mmol) was loaded into a tidy silica glass tube (Φ10 mm×100 mm) and the tube was flame-sealed under 10^{-3} Pa. The tube was heated to 380 °C in 3 h, and held at this temperature for 24 h, and then cooled to 30 °C with a rate of 1.0 °C /h. The single crystals of $Cs_4B_4O_3F_{10}$ crystals can also be synthesized by a high-temperature solution reaction with spontaneous nucleation technique in an open system. A mixture of CsF, $CsBF_4$, and H_3BO_3 was weighted under its stoichiometry. The samples were mixed in an agate mortar, and then moved to a platinum crucible, which were placed in the furnace assembled by us. The samples were gradually heated at the speed of 50 °C/h from room temperature to 350 °C and held at this temperature for 24 h, then cooled to 100 °C at a rate of 1 °C/h, after that, cooled to the room temperature at a rate of 5 °C/h. During the process of spontaneous crystallization, small single crystals were formed in the platinum crucible. The polycrystalline samples of $Cs_4B_4O_3F_{10}$ were synthesized via conventional solid-state reactions in an open system. The stoichiometric compositions are as follows: $CsBF_4$ (6.9 mmol, 1.521 g), CsF (6.9 mmol, 1.051 g), and H_3BO_3 (6.9 mmol, 0.428 g). The mixtures were ground thoroughly, placed in platinum crucibles, and gradually heated to 250 °C and held at this temperature in air for 24 h.

Characterization: Powder XRD data were collected with a Bruker D2 PHASER diffractometer (Cu Kα radiation with λ = 1.5418 Å, 2θ = 10 to 60°, scan step width = 0.02°, and counting time = 1 s/step). The single-crystal XRD data were collected on a Bruker D8 Venture diffractometer using Mo Kα radiation (λ = 0.71073 Å) at room temperature. The intensity, reduction and cell refinements were carried out on Bruker SAINT.[11] All the structures were solved by direct method and refined through the full-matrix least-squares fitting on F^2 with OLEX2 software.[12] These structures were verified by virtue of ADDSYM algorithm from PLATON.[13] Thermal gravimetric analysis (TGA) and differential scanning calorimetry (DSC) were carried out on a simultaneous NETZSCH STA 449 F3 thermal analyzer instrument in a flowing N2 atmosphere, the sample was placed in Pt crucible, heated from 40 to 400 °C at a rate of 5 °C min^{-1}. Infrared spectroscopy was carried out on a Shimadzu IR Affinity-1 Fourier transform infrared spectrometer in the 400–4000 cm^{-1} range. UV-vis-NIR diffuse-reflectance spectroscopy data in the wavelength range of 200–2500 nm were recorded at room temperature using a powder sample of $Cs_4B_4O_3F_{10}$ on a Shimadzu SolidSpec-3700 DUV spectrophotometer.

Calculation details: The electronic structure and the optical property were calculated by using the DFT method implemented in the CASTEP package.[14] During the calculation, the generalized gradient approximation (GGA) with Perdew-Burke-Ernzerhof (PBE) functional was adopted.[15] Under the norm-conserving pseudopotential (NCP), the following orbital electrons were treated as valence electrons: B:$2s^2 2p^1$, O:$2s^2 2p^4$, F:$2s^2 2p^4$, and Cs:$5s^2 5p^6 6s^1$. The kinetic energy cutoff of 940 eV was chosen, and the numerical integration of the Brillouin zone was performed using a 2×3×3 Monkhorst-Pack *k*-point sampling. The other calculation parameters and convergent criteria were the default values of the CASTEP code. The formation energy can be expressed by the following calculation formula:

$$E_{form} = (E_{compound} - \sum N_i E_{atom})/N$$

Where N_i is the number of different atoms in the related compound, $E_{compound}$ refers to the energy of corresponding compound, E_{atom} is the energy of individual atoms, and N is the total number of atoms in the compound.

Acknowledgements

We gratefully acknowledge the Xinjiang Key Laboratory of Electronic Information Materials and Devices (2020D04013), National Natural Science Foundation of China (52002397), Xinjiang Tianshan Youth Program-Outstanding Young Science and Technology Talents (2019Q026), the International Partnership Program of CAS (1A1365KYSB20200008), CAS President's International Fellowship Initiative (2020DC0006), the Science and Technology Service Network Initiative of CAS (KFJ-STS-QYZD-130), and the Western Light Foundation of CAS (Y92S191301).

Conflict of Interest

The authors declare no conflict of interest.

Keywords: Borates · congruently melting · fluorooxoborates · heteroanionic units · micro-symmetry

[1] a) H. Kageyama, K. Hayashi, K. Maeda, J. P. Attfield, Z. Hiroi, J. M. Rondinelli, K. R. Poeppelmeier, *Nat. Commun.* **2018**, *121*, 772; b) J. K. Harada, N. Charles, K. R. Poeppelmeier, J. M. Rondinelli, *Adv. Mater.* **2019**, *31*, 1805295–1805321; c) S. Bai, D. Wang, H. K. Liu, Y. Wang, *Inorg. Chem. Front.* **2021**, 8, 1637–1654.

[2] a) M. Mutailipu, K. R. Poeppelmeier, S. L. Pan, *Chem. Rev.* **2021**, *121*, 1130–1202; b) M. Mutailipu, M. Zhang, Z. H. Yang, S. L. Pan, *Acc. Chem. Res.* **2019**, *52*, 791–801; c) C. Chen, T. Sasaki, R. K. Li, Y. Wu, Z. S. Lin, Y. Mori, Z. G. Hu, J. Y. Wang, S. Uda, M. Yoshimura, Y. Kaneda, *Nonlinear Optical Borate Crystals*, Wiley-VCH Verlag & Co. KGaA, Boschstr. Weinheim, Germany, **2012**; d) M. Mutailipu, Z. H. Yang, S. L. Pan, *Acc. Mater. Res.* **2021**, *2*, 282–291; e) Q. Jing, G. Yang, Z. H. Chen, X. Y. Dong, S. Y. Jing, *Inorg. Chem.* **2018**, 57, 3, 1251–1258; f) X. R. Shi, Q. Jing, Z. H. Chen, M. H. Lee, H. M. Duan, H. Q. Ding, *J. Appl. Phys.* **2020**, *128*, 113103.

[3] a) S. G. Jantz, F. Pielnhofer, L. V. Wüllen, R. Weihrich, M. J. Schäfer, H. A. Höppe, *Chem. Eur. J.* **2018**, *24*, 443–450; b) T. Brauniger, T. Pilz, C. V. Chandran, M. Jansen, *J. Solid State Chem.* **2012**, *194*, 245–249; c) B. B. Zhang, G. Q. Shi, Z. H. Yang, F. F. Zhang, S. L. Pan, *Angew. Chem. Int. Ed.* **2017**, *56*, 3916–3919; *Angew. Chem.* **2018**, *130*, 3974–3977; d) M. Luo, F. Liang, Y. X. Song, D. Zhao, N. Ye, Z. S. Lin, *J. Am. Chem. Soc.* **2018**, *140*, 6509–6509; e) S. G. Jantz, M. Dialer, L. Bayarjargal, B. Winkler, L. van Wüllen, F. Pielnhofer, J. Brgoch, R. Weihrich, H. A. Höppe, *Adv. Opt. Mater.* **2018**, *6*, 1800497–1800505.

[4] a) G. Q. Shi, Y. Wang, F. F. Zhang, B. B. Zhang, Z. H. Yang, X. Hou, S. L. Pan, K. R. Poeppelmeier, *J. Am. Chem. Soc.* **2017**, *139*, 10645–10648; b) X. F. Wang, Y. Wang, B. B. Zhang, F. F. Zhang, Z. H. Yang, S. L. Pan, *Angew. Chem. Int. Ed.* **2017**, *56*, 14119–14123; *Angew. Chem.* **2017**, *129*, 14307–14311; c) Y. Wang, B. B. Zhang, Y. Z. H. Yang, S. L. Pan, *Angew. Chem. Int. Ed.* **2018**, *57*, 2150–2154; *Angew. Chem.* **2018**, *130*, 2172–2176; d) Z. Z. Zhang, Y. Wang, B. B. Zhang, Z. H. Yang, S. L. Pan, *Angew. Chem. Int. Ed.* **2018**, *57*, 6577–6581; *Angew. Chem.* **2018**, *130*, 6687–6691; e) M. Mutailipu, M. Zhang, B. B. Zhang, L. Y. Wang, Z. H. Yang, X. Zhou, S. L. Pan, *Angew. Chem. Int. Ed.* **2018**, *57*, 6095–6099; *Angew. Chem.* **2018**, *130*, 6203–6207; f) M. Xia, F. M. Li, M. Mutailipu, S. J. Han, Z. H. Yang, S. L. Pan, *Angew. Chem. Int. Ed.* **2021**, https://doi.org/10.1002/anie.202103657.

[5] a) C. Tao, R. K. Li, *Chem. Eur. J.* **2020**, *26*, 3709–3712; b) C. C. Tang, X. X. Jiang, W. L. Yin, L. J. Liu, M. J. Xia, Q. Huang, G. M. Song, X. Y. Wang, Z. S. Lin, C. T. Chen, *Dalton Trans.* **2019**, *48*, 21–24; c) M. Mutailipu, M. Zhang, B. B. Zhang, Z. H. Yang, S. L. Pan, *Chem. Commun.* **2018**, *54*, 6308–6311; d) T. Pilz, H. Nuss, M. Jansen, *J. Solid State Chem.* **2012**, *186*, 104–108; e) L. Y. Li, G. B. Li, Y. X. Wang, F. H. Liao, J. H. Lin, *Chem. Mater.* **2005**, *17*, 4174–4180.

[6] a) W. Y. Zhang, Z. L. Wei, Z. H. Yang, S. L. Pan, *Inorg. Chem.* **2020**, *59*, 3274–3280; b) M. Cheng, W. Q. Jin, Z. H. Yang, S. L. Pan, *Inorg. Chem.* **2020**, *59*, 13014–13018.

[7] a) S. G. Zhao, P. F. Gong, L. Bai, X. Xu, S. Q. Zhang, Z. H. Sun, Z. S. Lin, M. C. Hong, C. T. Chen, J. H. Luo, *Nat. Commun.* **2014**, *5*, 4019; b) G. Sohr, N. Ciaghi, M. Schauperl, K. Wurst, K. R. Liedl, H. Huppertz, *Angew. Chem. Int. Ed.* **2015**, *54*, 6360–6363; *Angew. Chem.* **2015**, *127*, 6458–6461; c) M. J. Xia, X. X. Jiang, Z. S. Lin, R. K. Li, *J. Am. Chem. Soc.* **2016**, *138*, 14190–14193; d) T. T. Tran, N. Z. Koocher, J. M. Rondinelli, P. S. Halasyamani, *Angew. Chem. Int. Ed.* **2017**, *56*, 2969–2973; *Angew. Chem.* **2017**, *129*, 3015–3019.

[8] a) J. H. Wang, Q. Wei, J. W. Cheng, H. He, B. F. Yang, G. Y. Yang, *Chem. Commun.* **2015**, *51*, 5066–5068; b) Q. Wei, J. J. Wang, C. He, J. W. Cheng, G. Y. Yang, *Chem. Eur. J.* **2016**, *31*, 10759–10762; c) F. Kong, S. P. Huang, Z. M. Sun, J. G. Mao, W. D. Cheng, *J. Am. Chem. Soc.* **2006**, *128*, 7750–7751; d) E. L. Belokoneva, *Crystallogr. Rev.* **2005**, *11*, 151–198; e) G. H. Zou, C. S. Lin, H. Jo, G. Nam, T. S. You, K. M. Ok, *Angew. Chem. Int. Ed.* **2016**, *55*, 12078–12082; *Angew. Chem.* **2016**, *128*, 12257–12261; f) C. D. McMillen, J. T. Stritzinger, J. W. Kolis, *Inorg. Chem.* **2012**, *51*, 3953–3955.

[9] a) A. J. Cresswell, S. G. Davies, P. M. Roberts, J. E. Thomson, *Chem. Rev.* **2015**, *115*, 566–611; b) M. A Miranda, H. Garcia, *Chem. Rev.* **1994**, *94*, 1063–1089. c) Crystal Data for $Cs_4B_4O_3F_{10}$: monoclinic, $P2_1/c$, $Z=4$, $a=15.4748(6)$ Å, $b=9.9990(4)$ Å, $c=9.6316(3)$ Å, $\beta=91.180(2)$ °, $F(000)=1416$, R_1 ($I>2$sigma(I))$=0.0257$, wR_2 ($I>2$sigma(I))$=0.0494$, R_1 (all data)$=0.0367$, wR_2 (all data)$=0.0526$. Further details of the crystal structure investigations discussed in this contribution are listed in Tables S1–S5 in the Supporting Information. Deposition Number(s) 2065508 contain(s) the supplementary crystallographic data for this paper. These data are provided free of charge by the joint Cambridge Crystallographic Data Centre and Fachinformationszentrum Karlsruhe Access Structures service www.ccdc.cam.ac.uk/structures.

[10] SAINT, Version 7.60 A, Bruker Analytical X-ray Instruments, Inc., Madison, WI, **2008**.

[11] O. V. Dolomanov, L. J. Bourhis, R. J. Gildea, J. A. K. Howard, H. Puschmann, *J. Appl. Crystallogr.* **2009**, *42*, 339–341.

[12] A. L. Spek, *J. Appl. Crystallogr.* **2003**, *36*, 7–13.

[13] S. J. Clark, M. D. Segall, C. J. Pickard, P. J. Hasnip, M. J. Probert, K. Refson, M. C. Payne, *Z. Anorg. Allg. Chem.* **2005**, *220*, 567–570.

[14] J. P. Perdew, K. Burke, M. Ernzerhof, *Phys. Rev. Lett.* **1996**, *77*, 3865–3868.

[15] J. M. K. Y Chan, G. Ceder, *Phys. Rev. Lett.* **2010**, *105*, 196403.

Manuscript received: April 13, 2021
Accepted manuscript online: May 3, 2021
Version of record online: ■■, ■■■

COMMUNICATION

A new congruently melting borate $Cs_4B_4O_3F_{10}$ has been synthesized as the first fluorooxoborate with $[BF_4]$ involving heteroanionic units, which possesses two highly fluorinated anionic clusters and therefore its formula can be expressed as $Cs_3(B_3O_3F_6)\cdot Cs(BF_4)$. More importantly, $Cs_4B_4O_3F_{10}$ shows the lowest melting point among all the available borates and thus sets a new record for such system.

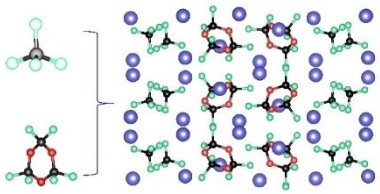

M. Xia, Prof. M. Mutailipu, F. Li, Prof. Z. Yang, Prof. S. Pan**